HHS Public Access

Author manuscript

Oncogene. Author manuscript; available in PMC 2023 March 27.

Published in final edited form as:

Oncogene. 2021 January ; 40(1): 215–231. doi:10.1038/s41388-020-01518-2.

Metabolic Programming of Distinct Cancer Stem Cells Promotes Organotropic Metastasis of Pancreatic Ductal Adenocarcinoma

Rama Krishna Nimmakayala[1], **Frank Leon**[1], **Satyanarayana Rachagani**[1], **Sanchita Rauth**[1], **Palanisamy Nallasamy**[1], **Saravanakumar Marimuthu**[1], **Gautam K. Shailendra**[1], **Yashpal S. Chhonker**[2], **Seema Chugh**[1], **Ramakanth Chirravuri**[1], **Rohitesh Gupta**[1], **Kavita Mallya**[1], **Dipakkumar R. Prajapati**[3], **Subodh M. Lele**[3], **Thomas Caffrey**[4], **Jean Grem**[4], **Paul M. Grandgenett**[4], **Michael A Hollingsworth**[4], **Pharm. D.J. Murry**[2], **Surinder K. Batra**[1,4,*], **Moorthy P. Ponnusamy**[1,4,*]

[1]Department of Biochemistry and Molecular Biology, College of Medicine, University of Nebraska Medical Center, Omaha, NE 68198-5870, USA.

[2]Department of Pharmacy Practice and Science, College of Pharmacy, University of Nebraska Medical Center, 986145 Nebraska Medical Center, Omaha, NE 68198-6145, USA.

[3]Department of Pathology and Microbiology, College of Medicine, University of Nebraska Medical Center, Omaha, NE, USA.

[4]Eppley Institute for Research in Cancer and Allied Diseases, Fred & Pamela Buffett Cancer Center, University of Nebraska Medical Center, Omaha, NE, USA.

Abstract

Pancreatic ductal adenocarcinoma (PDAC) metastasizes to distant organs, which is the primary cause of mortality; however, specific features mediating organ-specific metastasis remain unexplored. Emerging evidence demonstrates that cancer stem cells (CSCs) and cellular metabolism play a pivotal role in metastasis. Here, we investigated the role of distinct subtypes of pancreatic CSCs and their metabolomic signatures in the organ-specific metastatic colonization. We found that PDAC consists of ALDH+/CD133+ and drug-resistant (MDR1+) sub-types of CSCs with specific metabolic and stemness signatures. Human PDAC tissues with gemcitabine treatment, autochthonous mouse tumors from *Kras^{G12D}; Pdx1-Cre* (KC), and *Kras^{G12D}; Trp53^{R172H}; Pdx-1Cre* (KPC) mice, and KPC- Liver/Lung metastatic cells were used to evaluate the CSC, EMT (epithelial-to-mesenchymal transition), and metabolic profiles. A strong association was observed between distinct CSC subtypes and organ-specific colonization. The

[*]**Correspondence**: Moorthy P. Ponnusamy and Surinder K. Batra, Department of Biochemistry and Molecular Biology, University of Nebraska Medical Center, Omaha, Nebraska, 68198-5870, U.S.A. Phone: 402-559-1170, Fax: 402-559-6650, mpalanim@unmc.edu (M.P.P) and sbatra@unmc.edu (S.K.B).

Author contributions

M.P.P., S.K.B., and R.K.N. conceived and designed the experiments. R.K.N. performed the experiments. F.L., S.R., P.N., G.S.K., S.C., and R.G. assisted with *in vitro* experiments. S.R. and S.M. assisted with *in vivo* experiments. Y.S.C. assisted and performed mass spectrometry experiments. M.P.P., S.K.B., R.K.N., D.J.M., M.A.H., S.M.L., and P.D.R. analyzed the data. P.M.G. and M.A.H. collected and provided human specimens. R.K.N. and M.P.P. wrote the manuscript.

Additional methods can be found in the Supplementary Materials.

Conflicts of interest

SKB is one of the co-founders of Sanguine Diagnostics and Therapeutics, Inc. The other authors disclosed no potential conflicts of interest.

liver metastasis showed drug-resistant CSC- and EMT-like phenotype with aerobic glycolysis and fatty acid β-oxidation-mediated oxidative (glyco-oxidative) metabolism. On the contrary, lung metastasis displayed ALDH+/CD133+ and MET-like phenotype with oxidative metabolism. These results were obtained by evaluating FACS-based side population (SP), autofluorescence (AF+) and Alde-red assays for CSCs, and Seahorse based oxygen consumption rate (OCR), extracellular acidification rate (ECAR), and fatty acid β-oxidation (FAO)-mediated OCR assays for metabolic features along with specific gene signatures. Further, we developed *in vitro* human liver and lung PDAC metastasis models by using a combination of liver or lung decellularized scaffolds, a co-culture, and a sphere culture methods. The ***liver****-mimicking* model showed MDR1+ and CPT1A+ populations, while the *lung-mimicking* environment showed the enrichment of ALDH+/CD133+ populations. Additionally, we observed significantly elevated expression of ALDH1 in lung metastasis and MDR1/LDHA expression in liver metastasis compared to human primary PDAC tumors. Our studies elucidated that distinct CSCs adapt unique metabolic signatures for organotropic metastasis, which will pave the way for the development of targeted therapy for PDAC metastasis.

Introduction

Pancreatic ductal adenocarcinoma (PDAC) is one of the most intractable malignancies, being the seventh leading cause of global cancer-related mortality(1). The high mortality rate of PDAC is because cancer has often metastasized to distant organs (liver, lung, peritoneum, and lymph nodes) during clinical diagnosis. Thus far, mechanisms underlying metastasis in PDAC are poorly understood. In the last decade, several studies indicated that cancer stem cells (CSCs) in PDAC play a central role in tumorigenesis, drug resistance, aggressiveness, and metastasis(2–6). Different markers to detect CSCs in PDAC have been proposed(4–10); however, whether a specific marker identifies the same or distinct CSC populations is unclear. Studies in breast cancer and PDAC indicated that CSC populations differ in their energy metabolism and show metabolic heterogeneity(11, 12). Whether distinct CSC populations exist with specific metabolic signatures in PC is not clear(13, 14). Gemcitabine is one of the critical chemotherapy drugs utilized to treat PDAC. Cell clones with acquired gemcitabine resistance show increased glycolytic metabolism(15). Pancreatic tumors also consist of clones that are intrinsically resistant to gemcitabine(16). These findings raise the interesting question of whether the gemcitabine-resistant clones have stem cell features distinct from other CSC sub-clones.

Based on the “Seed” and “Soil” theory and a new theory by Schild et al., during the evolution of a specific cancer cell in a primary tumor, the cells acquire a metabolic signature that supports their future colonization in a particular organ(17). Lehuede et al., have proposed that only metabolically flexible cancer cells could survive in distant organs and form metastases(18). In other words, a metabolic match between “Seed” and “Soil” is essential for proper colonization and metastasis formation. Several studies(19–23) suggest that CSCs are among several metastasis-associated cell types in the PDAC. Based on these studies and the association of CSCs with metastasis, we hypothesize that distinct CSC populations with sub-type specific metabolic and stem cell features colonize and survive in a particular organ.

Here, we identified distinct subsets of CSCs with specific metabolic signatures in human and mouse pancreatic tumors. We observed a clear correlation among distinct CSC subtypes, their metabolism, and organ-specific colonization and metastasis. These distinct CSC populations also showed preference to colonize and survive in a specific organ (liver or lung) environment. The knowledge obtained from this study will be instrumental in developing organ-specific metastatic therapy for PDAC metastasis.

Results

ALDH1A1/CD133 and MDR1 identify distinct subtypes of CSC populations in PDAC tumors

Previous studies identified ALDH, CD133, and MDR1 as pancreatic CSC markers (4–7). Cancer cells expressing various stem cell markers, such as ALDH, CD133, side population (SP) or drug-resistant population, EpCAM, CD44, CD24, and intracellular autofluorescence (AF) exist in PDAC (Supplementary Fig. 1a–e) and show *in vivo* tumorigenic properties, involved in tumor progression and metastasis(7, 21, 23, 24). However, it is not clear whether these CSC markers identify the same or distinct pancreatic CSC populations. As revealed by immunofluorescence staining, ALDH- and MDR1-positive cells were identified mostly as distinct non-overlapping cell populations in pancreatic tumors obtained from patients without gemcitabine treatment (Figure 1a). However, pancreatic tumors with gemcitabine treatment showed a loss of ALDH1A1 and elevated expression of MDR1 (Figure 1a). Also, pancreatic tumors of $Kras^{G12D}$; Pdx-1 Cre (KC) mice showed distinct localization of ALDH and MDR1 CSC markers (Figure 1b). Interestingly, ALDH and CD133 identified the same subtype of the CSC population, as shown by immunofluorescence staining (Figure 1c). Based on this data, we categorized the pancreatic CSC population into two sub-types: ALDH+/CD133+ CSCs and MDR1+ CSCs. To further explore the functional features of these populations, we developed distinct in vitro CSC models as described in materials and methods. The Sph and Sph+Gem cells showed increased *in vivo* tumorigenic properties as compared to Adh cells (Supplementary Fig. 2). As assessed by flow cytometry, the percentage of side population (SP) was higher in the Sph+Gem population as compared to Adh and Sph populations (Figure 1e and h). In addition, the percentage of AF, an intracellular marker for CSCs (10, 25), was increased in Sph+Gem cells as compared to Sph cells (Figure 1f and h). The percentage of ALDH+ was higher in Sph cells than in the Sph+Gem population (Figure 1g and h). Analysis of CSC marker expression using qRT-PCR showed overexpression of CD133 and MDR1 in Sph and Sph+Gem populations, respectively (Figure 1i and j). Interestingly, KLF4, a pluripotent stem cell marker, was higher in Sph-derived cells, whereas the expression of CD44v9 was higher in Sph+Gem cells (Figure 1k). Together, these data identify distinct subtypes of CSC populations in pancreatic tumors with specific localization and stem cell features.

Distinct pancreatic CSC sub-type populations display specific metabolism

Metabolic gene expression analysis showed elevated expression of genes associated with aerobic glycolysis and oxidative phosphorylation in MiaPaCa-2 Sph+Gem cells, including c-Myc and PGC1α (Figure 2a). We also measured the extracellular acidification rate (ECAR) and oxygen consumption rate (OCR) in these CSC populations using a Seahorse extracellular flux analyzer and treating cells with various inhibitors of glycolysis and

oxidative phosphorylation. MiaPaCa-2 Sph+Gem cells showed increased ECAR, glycolysis, glucose uptake, and lactate release (Figure 2b–e). Interestingly, the Sph+Gem cells also showed increased OCR, suggesting that the drug-resistant CSCs are glyco-oxidative (Figure 2f and g). However, Sph cells showed increased OCR and decreased ECAR, glucose uptake, and lactate release (Figure 2b–g). LC-MS/MS metabolite analysis further confirmed these results by showing that the levels of glycolysis metabolites, including lactate (the end-product of the Warburg effect), are higher in drug-resistant cells (Figure 2h). As shown by immunofluorescence staining on pancreatic tumors from human PDAC patients and KC mice, MDR1-positive cells co-expressed with LDH-A, an enzyme that catalyzes the conversion of pyruvate to lactate (Warburg effect) (Figure 2i). Interestingly, cells expressing LDH-A did not show co-expression with ALDH1A1, suggesting that the ALDH+ population does not display the Warburg effect (Figure 2i). These results suggest that drug-resistant cells (Sph+Gem) are glyco-oxidative (intermediate metabolism), while Sph (ALDH+/CD133+) cells are oxidative.

β-oxidation of fatty acids contributes to oxidative phosphorylation in drug-resistant CSCs

Next, we investigated if β-oxidation of fatty acids contributes to the increased oxidative phosphorylation in drug-resistant cells, as most of the pyruvate is converted into lactate through aerobic glycolysis (Warburg effect) in these resistant cells. We analyzed the expression of CPT1A and MDR1 in PDAC tissues and found they were coexpressed (Figure 2j). To examine whether the drug-resistant subtype of CSCs shows FAO-mediated oxidative phosphorylation, we measured the oxidation of fatty acids and OCR in response to etomoxir, an inhibitor of FAO using the XF Palmitate-BSA FAO Substrate with the XF Cell Mito Stress Test and the Seahorse extracellular flux analyzer. Treatment with etomoxir inhibited OCR only in the Sph+Gem population, suggesting FAO increases maximal OCR in drug-resistant CSCs (Figure 2k). To further confirm this, we sorted SP CD133- (drug-resistant CSCs), CD133+ NSP (CD133+ CSCs), and NSP CD133- (non-CSCs) from the SUIT-2 PDAC cell line using FACS (Supplementary Fig. 3a–d) and analyzed FAO gene expressions. As expected, the drug-resistant CSCs showed increased expression of CPT1A, CPT2, CPT1C, ACADM, ACADL, ACAD9, ACAD11, and ECI1 compared to non-CSCs and Sph cells (Figure 2l). Similar results were also observed in MiaPaCa-2 Sph+Gem cells (Figure 2m). These results suggest that the oxidative phosphorylation in drug-resistant cells is due to FAO.

Liver and lung metastases of PDAC show specific stem cell features

Growing evidence suggests that CSCs show metastatic features, and the presence of stem-like circulating tumor cells (CTCs) in blood further strengthens this notion(2, 21–23, 26). We found that distinct pancreatic CSC populations showed differential migratory potentials (Supplementary Fig. 4). The CTCs in patients with colorectal cancer or PDAC showed CSC features, suggesting that CSCs are associated with the metastasis process(27, 28). Several recent studies also provide evidence for the propensity of different CSCs to metastasize to a specific organ. Therefore, we asked whether liver and lung metastases of PDAC (predominant metastatic sites) show specific stem cell features. To this end, we first analyzed mRNA expression profiles of ALDH1A1, ALDH1A3, PROM1, and ABCB1 in human primary and metastatic lesions using the GSE34153 data set (Figure

3a). Lung metastasis showed increased ALDH1A1 and PROM1, while liver metastasis showed elevated ABCB1 expression (Figure 3a). To further explore the stemness features of organ-specific metastasis, we developed $Kras^{G12D}$; $Trp53^{R172H}$; Pdx-1Cre (KPC) primary (Panc78) and metastatic (Liver78 and Lung78) cell lines from KPC mouse of age 20 weeks (Supplementary Fig. 5a). The Panc78, Lung78, and Liver78 cell lines were characterized by morphologically (Supplementary Fig. 5b). Further, these cells showed a differential of Vimentin and proliferation potentials (Supplementary Fig. 5c). The ductal feature of these cell lines was confirmed by the expression of CK19 (Supplementary Fig. 5c). KPC liver metastasis (Liver78) shows increased SP and AF (Figure 3b–e), while KPC lung metastasis (Lung78) shows an increased CD133+ population (Figure 3f and g). The mRNA expression levels of Aldh1a1 and Prom1 were higher in KPC lung metastasis, whereas the expression of Abcb1a was higher in KPC liver metastasis (Figure 3h). In addition, the KPC-liver and -metastatic lung cells showed differential expression of pluripotent and stem cell markers (Sox2, Sox9, Nanog, and Oct3/4) expressions as compared to primary KPC tumor cells (Panc78) (Supplementary Fig. 6). KPC-liver and -lung metastatic cells showed increased sphere formation, which suggests elevated stemness properties of metastatic cells (Figure 3i and j). Immunofluorescence staining also showed increased ALDH1A1/CD133 staining in KPC-lung metastasis, while higher MDR1 staining occurred in KPC-liver metastasis. The spontaneous lung metastasis PDAC cell line, S2-VP10 showed a significant increase in CD133 expression (Supplementary Fig. 7), while the spontaneous liver metastasis cell line, L3.6pL, showed a significant increase in ABCB1 expression and drug-resistant features such as intracellular AF and SP as compared to a non-metastatic cell line, MiaPaCa-2 (Supplementary Fig. 8). These results suggest that liver and lung metastases of PDAC display organ-specific stem cell features.

Liver and lung metastases of PDAC show specific metabolic signatures

Next, we analyzed mRNA expression profiles of genes that encode glycolysis, TCA cycle, and oxidative phosphorylation proteins in human primary and metastatic lesions using the same GSE34153 data set as mentioned in Figure 3a. PDAC liver metastasis showed increased expression of glycolytic genes, including MYC, PDK1, and LDHA (Figure 4a). Furthermore, we observed increased expression of the TCA cycle and oxidative phosphorylation genes in PDAC liver metastasis (Figure 4b and c). We further validated these results using an extracellular flux analyzer, which showed that ECAR, glycolytic capacity, and OCR are higher in KPC-liver metastasis compared to KPC-lung metastasis (Figure 4d, e, and f). However, KPC-lung metastasis showed an elevated OCR but decreased ECAR (Figure 4d, e, and f). KPC-liver metastasis expressed higher Cpt1b levels (Figure 4g). We observed similar results with spontaneous liver and lung tropic metastasis cells, L3.6pL and S2-VP10 (Supplementary Fig. 9 and 10). Lung tropic cells showed an increased OCR, while liver tropic cells showed an elevated ECAR and OCR (Supplementary Fig. 9a–c). mRNA expression levels of glycolytic and oxidative genes were higher in liver tropic cells as compared to S2-VP10 and MiaPaCa-2; however, the mRNA levels for the glycolytic gene were lower in S2-VP10 as compared to L3.6pL and MiaPaCa-2. Overall, our results indicate that liver metastasis shows a glyco-oxidative metabolic signature, and lung metastasis shows an oxidative signature. Interestingly, similar to drug-resistant CSCs, human PDAC liver metastasis also showed increased mRNA expression of genes that encode

fatty acid β-oxidation proteins (Figure 4h). An etomoxir treatment could reduce maximal OCR only in KPC-liver metastasis (Figure 4i). Through our immunofluorescent staining, we observed increased co-expression of CPT1A with MDR1, but not with ALDH1A1 in KPC-liver metastasis compared to KPC-lung metastasis (Figure 4j).

Lung and liver metastasis of PDAC show specific EMT/MET features

Next, we sought to examine whether lung and liver metastases of PDAC show organ-specific EMT/MET features. We observed an increased percentage of Epcam+ cells in KPC-lung metastasis as compared to KPC-liver metastasis, as analyzed by flow cytometry (Figure 5a and b). Further validation with qRT-PCR showed increased expression levels of EMT genes, such as Zeb1, Snai2, Cdh2, and vimentin in KPC-liver metastasis (Figure 5c). In contrast, decreased expression of EMT genes and elevated expressions of MET genes, such as Cdh1 and Epcam, were observed in KPC-lung metastasis (Figure 5c). MiaPaCa-2 Sph+Gem cells also showed a significant increase in the expression of the mesenchymal gene, Zeb1. Similar results were also observed in primary cell line models of KPC liver and lung metastases (Figure 5d). Further validation of these results using flow cytometry showed that the Epcam+ (MET) cells are mostly CD133+ CSC, while Epcam− (EMT) cells are drug-resistant CSCs (Figure 5e–h). Also, KPC-liver metastasis showed increased immunofluorescent staining for N-cadherin, vimentin, and CPT1A expression, while KPC-lung metastasis showed elevated staining for EpCAM, E-cadherin, and CD133 (Figure 5i and j). Thus, liver metastasis or drug-resistant pancreatic CSCs show EMT-like features, and lung metastases or ALDH+/CD133+ pancreatic CSCs show MET-like properties.

Distinct pancreatic CSC subtype populations show increased survival and enrichment in organ-specific metastatic *in vitro* environments

Our next goal was to investigate whether a pancreatic CSC sub-type with a specific metabolic signature could colonize and survive in a specific organ. To study this, we developed *in vitro* liver and lung PDAC metastasis models by using a combination of liver or lung decellularized scaffolds, a co-culture method, and a sphere culture method by following the protocols developed by Ramamoorthy et al. (29) with modifications as described in the supplementary materials and methods. Immunofluorescence staining showed the enrichment of MDR1+ cells with CPT1A expression in the liver-mimicking environment, while the ALDH+/CD133+ cell population was enriched in the lung environment (Figure 6f and g). Also, distinct CSC sub-type populations (GFP labeled Adh, Sph, and Sph+Gem cells of MiaPaCa-2) were seeded along with organ-specific cells as described above in ultra-low attachment plates. After one week of culture, single cells were stained with propidium iodide (to exclude dead cells) and analyzed for the percentage of GFP+ cells in each group. The percentage of Sph+Gem GFP+ cells was higher in the liver mimicking environment, while the Sph GFP+ cell percentage was higher in the lung environment (Figure 6h). Also, after one week of a culture of MiaPaCa-2 GFP+ cells in the above 3D culture conditions, single cells from 3D spheroids were analyzed for SP using flow cytometry. The MiaPaCa-2 GFP+ cells grown in the liver environment showed an increased percentage of SP (Figure 6i and j). As a final validation of these observations, we investigated the expression levels of stem cell and metabolic markers using immunohistochemistry in the human primary pancreatic tumor, lung metastasis, and liver metastasis tissues (n = 8; Figure 7). Analysis of these

tumor sections showed an elevated expression of ALDH1A1 in lung metastasis compared to liver metastasis and primary tumor (Figure 7a). In contrast, MDR1 and LDHA expression levels were higher in liver metastasis as compared to the primary tumor and lung metastasis (Figure 7a and b).

Discussion

CSCs are critical players of tumor growth and metastasis in PDAC(2, 5). Emerging evidence suggests that CSCs in the pancreatic tumor are heterogeneous with tumorigenic and metastatic properties(2, 5, 23, 30, 31). Studies in breast and PDAC indicate that CSC populations differ in their energy metabolism (11, 12). Interestingly, metastasis in multiple organs has different metabolic requirements to generate energy(32–35). However, it is not clear whether distinct CSC subtype populations with subtype-specific stem cell and metabolic signatures show organ-specific colonization. Here, we showed that PDAC comprises distinct subtypes of CSCs—ALDH+/CD133+ and MDR1+—with specific stem cell and metabolic profiles. We observed a significant correlation between one particular subtype of the CSC population and organ-specific metastasis. We demonstrated that lung metastasis shows an ALDH+/CD133+ CSC phenotype, oxidative metabolism, and MET-like phenotype. In contrast, liver metastasis shows a drug-resistant phenotype, glyco-oxidative metabolism, and EMT-like phenotype. We also observed preferential colonization of these distinct CSC populations in a specific organ.

Several recent studies have proposed different markers for detecting CSCs in solid tumors(4–10). However, it is not clear whether these markers identify the same or distinct CSC populations. If distinct sub-types of CSC populations exist, the functional differences among these subtypes are not apparent. Our findings suggest that pancreatic tumors consist of ALDH+/CD133+ CSCs and MDR1+ (drug-resistant) CSCs, each with distinct *in vivo* tumorigenic properties. Importantly, ALDH and CD133 identified the same subset of pancreatic CSCs. Furthermore, ALDH+/CD133+ pancreatic CSCs are $CD44^{Low}$ cells, while the drug-resistant CSCs are $CD44^{High}$. Our data and previous studies also indicate that a small percentage of the drug-resistant (MDR1+) population already exists in pancreatic tumors before therapy (6, 23, 36), and gemcitabine treatment further enriches the drug-resistant population by inhibiting ALDH+ CSCs. This further strengthens the distinction between these two pancreatic CSC sub-type populations.

In this study, we found that multiple subtypes of pancreatic CSCs show different metabolic signatures. Recently, a few studies demonstrated that CSCs exhibit differential metabolomic profiles. While several recent studies suggest the glycolytic dependency of CSCs(37–39), other studies showed that the CSCs rely on oxidative metabolism(11),(12, 40–42). These discrepant conclusions about CSC metabolism pose important questions about whether distinct sub-types of pancreatic CSCs maintain unique sub-type-specific metabolic signatures? Our study revealed that ALDH+/CD133+ pancreatic CSCs show oxidative metabolism, whereas MDR1+ drug-resistant pancreatic CSCs show both aerobic glycolysis and oxidative phosphorylation (glyco-oxidative). If drug-resistant pancreatic CSCs convert pyruvate to lactate through the Warburg effect, what substrate contributes to the oxidative phosphorylation in these CSCs? We identified β-oxidation of fatty acids as an essential

contributor to the oxidative phosphorylation in drug-resistant CSCs. In agreement with this, radio-resistant breast CSCs showed increased levels of CPT1A/CPT2, rate-limiting enzymes for mitochondrial fatty acid transportation and FAO, and inhibiting CPT1A/CPT2 attenuated FAO, reducing tumor growth and radiation resistance(43). Besides, FAO is essential for the chemoresistance of breast CSCs(44). We also observed that CPT1A and CPT1B levels are higher in drug-resistant pancreatic CSCs. Thus, we propose that distinct subtypes of pancreatic CSCs show specific metabolic signatures.

We observed that the metastasis in a specific organ shows organ-specific stem cell and metabolic signatures. Our findings and previous studies indicate that CSC populations are several metastasis-associated cell types (21–23). According to the “Seed” and “Soil” theory, cancer cells within the primary tumor show a preference for colonizing a specific distant organ. Several recent studies also provide evidence for the organ-specific metastatic abilities of CSCs in various cancers(45, 46). Moreover, cancer cells within tumors acquire a specific metabolic profile during evolution that allows them to survive in a specific distant organ(17). These theories, previous studies, and our observations prompted us to investigate whether the distinct pancreatic CSC sub-types exhibit organ-specific colonization and metastasis. We observed that the lung metastasis and spontaneous lung tropic cells of PDAC show an ALDH+/CD133+ CSC phenotype. In contrast, liver metastasis and spontaneous liver tropic metastatic cells display a drug-resistant phenotype. Interestingly, lung metastasis and lung tropic cells showed oxidative phosphorylation, whereas liver metastasis and liver tropic cells showed aerobic glycolysis and FAO-mediated oxidative metabolism (glyco-oxidative). Additionally, lung and liver metastases showed MET-like and EMT-like phenotypes, respectively. In agreement with this, EMT-like (CD44+CD24-) and MET-like (ALDH+) breast CSCs with glycolytic and oxidative metabolism, respectively, were described in the previous study(11). These observations link distinct sub-types of pancreatic CSCs with organ-specific PDAC metastasis. The metabolic program in a specific metastasizing cancer cell needs to be compatible with the metabolic environment of its target organ for proper colonization and metastasis formation(17). The liver environment has increased glycolysis, hypoxia, and FAO; therefore, an infiltrating cancer cell must be able to generate ATP from glycolysis and FAO to colonize and survive in the liver(17, 47, 48). In contrast, the lung is full of oxygen and oxidative stress, so a lung-colonizing cancer cell must be oxidative to overcome the oxidative barrier and survive in the lung(17). Our observations are in clear consensus with these notions and suggest that cancer cells, including CSCs within pancreatic tumors, may randomly disseminate; however, only those that metabolically match with the distant site will colonize, survive, and develop a metastasis. To prove this concept, we grew pancreatic cancer cells and distinct pancreatic CSC populations in culture environments mimicking the human liver and lung. ALDH+/CD133+ pancreatic CSCs grew better in the lung-mimicking environment, but the drug-resistant population survived better in the liver. Overall, these data suggest that distinct subtypes of CSCs show organ-specific colonization, survival, and metastatic potential. In summary, we identified distinct and metabolically varying pancreatic CSC populations and delineated their relation to organ-specific metastasis. Further investigation of the mechanism by which a specific metabolism in a pancreatic CSC contributes to its metastasis in a specific organ may illuminate our understanding of CSC organ-specific metastasis.

Materials and methods

Animals

All animal experiments were performed in compliance with procedures approved by the IACUC at the University of Nebraska Medical Center (UNMC). $Kras^{G12D}$; $Trp53^{R172H}$; Pdx-1Cre (KPC) and $Kras^{G12D}$; Pdx-1Cre (KC) animals were used in this study.

Human specimens

Human primary tumor, liver metastasis, and lung metastasis specimens from decedents who have previously been diagnosed with PDAC were obtained from UNMC's Tissue Bank through the Rapid Autopsy Program (RAP) for Pancreas in compliance with IRB 091–01. To ensure specimen quality, organs were harvested within three hours post-mortem, and the specimens were flash-frozen in liquid nitrogen or placed in formalin for immediate fixation. Sections were cut from paraffin blocks of formalin-fixed tissue into 4 μm-thick sections and mounted on charged slides. To prepare biomatrix scaffolds for the development of "3D *in vitro* liver and lung metastasis models", human fresh and healthy liver and lung tissues were obtained from the RAP at UNMC.

Cell lines

Cell lines were purchased from ATCC (MiaPaCa-2 (catalog number ATCC® CRL-1420), BEAS-2B (ATCC® CRL-9609™), MRC-5 (ATCC® CCL-171™), HUVEC (ATCC® PCS-100-010™), and CFPAC-1 (ATCC® CRL-1918)). Human immortalized hepatocytes, Fa2N-4 (Cat# IFH15), MFE support medium, and MFE plating medium were purchased from XenoTech LLC (Lenexa, KS). S2-VP10 cells were a kind gift from Dr. Ashok K. Saluja, University of Miami, USA. SUIT-2, and L3.6pL cells were a kind gift from Dr. Michel Ouellette, UNMC. The LX-2 cell line was a kind gift from Prof. Scott L Friedman, MD., Dean for Therapeutic Discovery and Chief of the Division of Liver Diseases at the Icahn School of Medicine at Mount Sinai, NY, USA. All cell lines were authenticated and verified as mycoplasma free every month. MiaPaCa-2, SUIT2, and S2-VP10 were grown adherently in Dulbecco's modified Eagle's medium (4.5 mg/mL glucose), supplemented with 10% fetal bovine serum and antibiotics (100 units/mL penicillin and 100 μg/mL streptomycin). The culture medium for the BEAS-2B cell line was purchased from Lonza (Lonza Cat# CC-3170). The MRC5 cell line was maintained in ATCC-formulated Eagle's Minimum Essential Medium (ATCC Cat# 30–2003) supplemented with 10% fetal bovine serum and antibiotics (100 units/mL penicillin and 100 μg/mL streptomycin). The HUVEC cell line was cultured in Vascular Cell Basal Medium (ATCC® PCS-100-030™) supplemented with the components of Endothelial Cell Growth Kit-BBE (ATCC® PCS-100-040™). The LX-2 cell line was cultured in Dulbecco's modified Eagle's medium (4.5 mg/mL glucose), supplemented with 2% fetal bovine serum and antibiotics (100 units/mL penicillin and 100 μg/mL streptomycin). Cells were incubated in a humidified incubator at 37 °C and supplied with 5% CO_2. We established primary PDAC and metastatic cell lines from KPC animals. KPC cell lines were isolated from KPC mouse of age 20 weeks. We harvested pancreatic tumor (Panc78), metastatic liver spots (Liver78), and metastatic lung spots (Lung78). Briefly, we chopped and minced the tissues and dissolved in RPMI containing liberase (1 mg/ml) for 30 min in a water bath at 37 C. Following

tissue solubilization, cells were passed through single-cell strainer and cultured till 10 passages. Differential trypsinization was performed at each passage to specifically select ductal PC cells by avoiding other cell contaminations such as fibroblasts. These cell lines were used at less than passage 15. These primary cell lines were grown adherently in RPMI medium supplemented with 10% fetal bovine serum and antibiotics (100 units/mL penicillin and 100 μg/mL streptomycin). For sphere culture, cells were cultured in stem cell medium: DMEM/F12 (Invitrogen, Grand Island, NY) medium supplemented with 1% B27, epidermal growth factor (20 ng/mL), and basic fibroblast growth factor (10 ng/mL). In some experiments, cells (2000/well) were plated in 96-well low-attachment culture plates in 200 μL of the stem cell medium. The number of spheres (Φ >100 μm) for each well was evaluated after ten days of culture. Images were captured using the EVOS FL Auto Imaging System (Thermo Fisher Scientific). MiaPaCa-2 cells were grown under sphere culture conditions in stem cell medium in the presence and absence of gemcitabine (3 μM) to generate drug-sensitive and drug-resistant CSC populations, respectively. MiaPaCa-2 cells cultured under adherent culture conditions using 10% DMEM were utilized as differentiated non-CSC control cells.

Development of distinct *in vitro* CSC models

A sphere culture method, which was described previously[12], was used to develop these models. Our preliminary data (Figure 1a) and previous studies have shown that a small percentage of the MDR1+ population exclusively exists in pancreatic tumors and was further enriched with gemcitabine treatment[6, 23, 24]. Therefore, we used gemcitabine ‘treatment’ to develop a drug-resistant subtype of pancreatic CSCs *in vitro*. MiaPaCa-2, a non-metastatic PDAC cell line, and Panc78, a primary pancreatic autochthonous tumor cell line from mouse KPC, were enriched using gemcitabine treatment to obtain resistant clones. The parental cells and gemcitabine-resistant were grown as spheres and denoted as “Sph” and “Sph+Gem”, respectively. MiaPaCa-2 or Panc78 cells grown as adherent cultures were considered non-CSC populations and denoted as “Adh” (Figure 1d).

Immunohistochemistry

Human PDAC tissues of primary, liver metastasis, and lung metastasis were obtained from the RAP for Pancreas at UNMC. Tissues were fixed and embedded in paraffin. Tissue sections were subjected to immunohistochemical staining by using the following primary antibodies at the indicated dilution: LDHA, 1:200 (Cell Signaling Technology Cat# 3582S), ALDH1A1, 1:100 (Santa Cruz Cat# Sc 374149), and MDR1, 1:100 (Santa Cruz Cat# Sc 55510). Antigen retrieval was performed in 10 mM sodium citrate buffer (pH 6). The stained sections were scored by Dr. Dipak Kumar Prajapati and Dr. Subodh M. Lele (Pathologists, UNMC), and intensity of ALDH1A1, MDR1, and LDHA expression was graded on a scale of 0 to 3 (0, no staining; 1+, weakly positive; 2+, moderately positive; 3+, strongly positive). The percentage of ALDH1A1, MDR1, and LDHA-positive staining were scored in a range of (0–100% or 0–1). A histoscore was calculated by multiplying intensity (0–3) and positivity (0–1), ranging between 0 and 3. GraphPad Prism software was used to calculate *P* values and to design graphs.

Supplementary Material

Refer to Web version on PubMed Central for supplementary material.

Acknowledgements:

We thank Craig Semerad, Victoria B. Smith, and Samantha Wall of the Flow Cytometry Research Facility, University of Nebraska Medical Center, for assisting with flow cytometry. We thank Janice A. Taylor and James R. Talaska of the Advanced Microscopy Core Facility at the University of Nebraska Medical Center for assisting with confocal microscopy. Also, we thank Dr. Kelly Stauch, Seahorse Core director at the University of Nebraska Medical Center, for assisting with Seahorse experiments. Funding: The authors in this article were supported primarily by the following grants from the National Institutes of Health P01 CA217798, R01 CA210637, R01 CA183459, R01 CA195586, R01 CA201444, R01 CA228524, U01 CA200466, R01 CA228524 and U01 CA210240, and the Nebraska Department of Health and Human Services LB595.

Abbreviations:

PDAC	Pancreatic ductal adenocarcinoma
CSCs	cancer stem cells
Shr	tumorsphere
ECAR	extracellular acidification rate
OCR	oxygen consumption rate
SP	side population
AF	autofluorescence
EMT	epithelial-to-mesenchymal transition
MET	Mesenchymal-to-e[ithelial transition
KPC	$Kras^{G12D}$ $Trp53^{R172H}$ Pdx-1Cre
KC	KrasG12D, Pdx-1Cre
RAP	Rapid Autopsy Program

References

1. Rawla P, Sunkara T, Gaduputi V. Epidemiology of Pancreatic Cancer: Global Trends, Etiology and Risk Factors. World J Oncol 2019;10(1):10–27. [PubMed: 30834048]
2. Hermann PC, Huber SL, Herrler T, Aicher A, Ellwart JW, Guba M, et al. Distinct populations of cancer stem cells determine tumor growth and metastatic activity in human pancreatic cancer. Cell Stem Cell 2007;1(3):313–23. [PubMed: 18371365]
3. Huang P, Wang CY, Gou SM, Wu HS, Liu T, Xiong JX. Isolation and biological analysis of tumor stem cells from pancreatic adenocarcinoma. World J Gastroenterol 2008;14(24):3903–7. [PubMed: 18609717]
4. Li C, Heidt DG, Dalerba P, Burant CF, Zhang L, Adsay V, et al. Identification of Pancreatic Cancer Stem Cells. Cancer Research 2007;67(3):1030–7. [PubMed: 17283135]
5. Li C, Lee CJ, Simeone DM. Identification of human pancreatic cancer stem cells. Methods Mol Biol 2009;568:161–73. [PubMed: 19582426]

6. Niess H, Camaj P, Renner A, Ischenko I, Zhao Y, Krebs S, et al. Side population cells of pancreatic cancer show characteristics of cancer stem cells responsible for resistance and metastasis. Target Oncol 2015;10(2):215–27. [PubMed: 24950733]
7. Kim MP, Fleming JB, Wang H, Abbruzzese JL, Choi W, Kopetz S, et al. ALDH Activity Selectively Defines an Enhanced Tumor-Initiating Cell Population Relative to CD133 Expression in Human Pancreatic Adenocarcinoma. PLOS ONE 2011;6(6):e20636. [PubMed: 21695188]
8. Klonisch T, Wiechec E, Hombach-Klonisch S, Ande SR, Wesselborg S, Schulze-Osthoff K, et al. Cancer stem cell markers in common cancers - therapeutic implications. Trends Mol Med 2008;14(10):450–60. [PubMed: 18775674]
9. Marcato P, Dean CA, Pan D, Araslanova R, Gillis M, Joshi M, et al. Aldehyde dehydrogenase activity of breast cancer stem cells is primarily due to isoform ALDH1A3 and its expression is predictive of metastasis. Stem Cells 2011;29(1):32–45. [PubMed: 21280157]
10. Miranda-Lorenzo I, Dorado J, Lonardo E, Alcala S, Serrano AG, Clausell-Tormos J, et al. Intracellular autofluorescence: a biomarker for epithelial cancer stem cells. Nat Methods 2014;11(11):1161–9. [PubMed: 25262208]
11. Luo M, Shang L, Brooks MD, Jiagge E, Zhu Y, Buschhaus JM, et al. Targeting Breast Cancer Stem Cell State Equilibrium through Modulation of Redox Signaling. Cell metabolism 2018;28(1):69–86.e6. [PubMed: 29972798]
12. Sancho P, Burgos-Ramos E, Tavera A, Bou Kheir T, Jagust P, Schoenhals M, et al. MYC/PGC-1alpha Balance Determines the Metabolic Phenotype and Plasticity of Pancreatic Cancer Stem Cells. Cell metabolism 2015;22(4):590–605. [PubMed: 26365176]
13. Menendez JA, Corominas-Faja B, Cuyàs E, Alarcón T. Metabostemness: Metaboloepigenetic reprogramming of cancer stem-cell functions. Oncoscience 2014;1(12):803–6. [PubMed: 25621295]
14. Menendez JA, Alarcón T. Metabostemness: a new cancer hallmark. Frontiers in oncology 2014;4:262-. [PubMed: 25325014]
15. Shukla SK, Purohit V, Mehla K, Gunda V, Chaika NV, Vernucci E, et al. MUC1 and HIF-1alpha Signaling Crosstalk Induces Anabolic Glucose Metabolism to Impart Gemcitabine Resistance to Pancreatic Cancer. Cancer Cell 2017;32(1):71–87.e7. [PubMed: 28697344]
16. Akada M, Crnogorac-Jurcevic T, Lattimore S, Mahon P, Lopes R, Sunamura M, et al. Intrinsic chemoresistance to gemcitabine is associated with decreased expression of BNIP3 in pancreatic cancer. Clin Cancer Res 2005;11(8):3094–101. [PubMed: 15837765]
17. Schild T, Low V, Blenis J, Gomes AP. Unique Metabolic Adaptations Dictate Distal Organ-Specific Metastatic Colonization. Cancer Cell 2018;33(3):347–54. [PubMed: 29533780]
18. Lehuede C, Dupuy F, Rabinovitch R, Jones RG, Siegel PM. Metabolic Plasticity as a Determinant of Tumor Growth and Metastasis. Cancer Res 2016;76(18):5201–8. [PubMed: 27587539]
19. Hoshino A, Costa-Silva B, Shen TL, Rodrigues G, Hashimoto A, Tesic Mark M, et al. Tumour exosome integrins determine organotropic metastasis. Nature 2015;527(7578):329–35. [PubMed: 26524530]
20. Rubin MA. Insights into the mechanism of organ-specific cancer metastasis. Cancer discovery 2014;4(11):1262–4. [PubMed: 25367948]
21. Liou G-Y. CD133 as a regulator of cancer metastasis through the cancer stem cells. The International Journal of Biochemistry & Cell Biology 2019;106:1–7. [PubMed: 30399449]
22. Celia-Terrassa T, Jolly MK. Cancer Stem Cells and Epithelial-to-Mesenchymal Transition in Cancer Metastasis. Cold Spring Harbor perspectives in medicine 2019.
23. Bhagwandin VJ, Bishop JM, Wright WE, Shay JW. The Metastatic Potential and Chemoresistance of Human Pancreatic Cancer Stem Cells. PLoS One 2016;11(2):e0148807. [PubMed: 26859746]
24. Rasheed ZA, Yang J, Wang Q, Kowalski J, Freed I, Murter C, et al. Prognostic significance of tumorigenic cells with mesenchymal features in pancreatic adenocarcinoma. J Natl Cancer Inst 2010;102(5):340–51. [PubMed: 20164446]
25. Nimmakayala RK, Seshacharyulu P, Lakshmanan I, Rachagani S, Chugh S, Karmakar S, et al. Cigarette Smoke Induces Stem Cell Features of Pancreatic Cancer Cells via PAF1. Gastroenterology 2018;155(3):892–908.e6. [PubMed: 29864419]

26. Charafe-Jauffret E, Ginestier C, Iovino F, Wicinski J, Cervera N, Finetti P, et al. Breast cancer cell lines contain functional cancer stem cells with metastatic capacity and a distinct molecular signature. Cancer Res 2009;69(4):1302–13. [PubMed: 19190339]
27. Grillet F, Bayet E, Villeronce O, Zappia L, Lagerqvist EL, Lunke S, et al. Circulating tumour cells from patients with colorectal cancer have cancer stem cell hallmarks in ex vivo culture. Gut 2017;66(10):1802–10. [PubMed: 27456153]
28. Poruk KE, Blackford AL, Weiss MJ, Cameron JL, He J, Goggins M, et al. Circulating Tumor Cells Expressing Markers of Tumor-Initiating Cells Predict Poor Survival and Cancer Recurrence in Patients with Pancreatic Ductal Adenocarcinoma. Clin Cancer Res 2017;23(11):2681–90. [PubMed: 27789528]
29. Ramamoorthy P, Thomas SM, Kaushik G, Subramaniam D, Chastain KM, Dhar A, et al. Metastatic Tumor-in-a-Dish, a Novel Multicellular Organoid to Study Lung Colonization and Predict Therapeutic Response. Cancer Res 2019;79(7):1681–95. [PubMed: 30674533]
30. Duong HQ, You KS, Oh S, Kwak SJ, Seong YS. Silencing of NRF2 Reduces the Expression of ALDH1A1 and ALDH3A1 and Sensitizes to 5-FU in Pancreatic Cancer Cells. Antioxidants (Basel) 2017;6(3).
31. Nimmakayala RK, Batra SK, Ponnusamy MP. Unraveling the journey of cancer stem cells from origin to metastasis. Biochimica et Biophysica Acta (BBA) - Reviews on Cancer 2019;1871(1):50–63. [PubMed: 30419314]
32. Mashimo T, Pichumani K, Vemireddy V, Hatanpaa KJ, Singh DK, Sirasanagandla S, et al. Acetate is a bioenergetic substrate for human glioblastoma and brain metastases. Cell 2014;159(7):1603–14. [PubMed: 25525878]
33. LeBleu VS, O'Connell JT, Gonzalez Herrera KN, Wikman H, Pantel K, Haigis MC, et al. PGC-1α mediates mitochondrial biogenesis and oxidative phosphorylation in cancer cells to promote metastasis. Nat Cell Biol 2014;16(10):992–15. [PubMed: 25241037]
34. Lin Y-H, Wu M-H, Huang Y-H, Yeh C-T, Cheng M-L, Chi H-C, et al. Taurine up-regulated gene 1 functions as a master regulator to coordinate glycolysis and metastasis in hepatocellular carcinoma. Hepatology 2018;67(1):188–203. [PubMed: 28802060]
35. Jiao L, Zhang H-L, Li D-D, Yang K-L, Tang J, Li X, et al. Regulation of glycolytic metabolism by autophagy in liver cancer involves selective autophagic degradation of HK2 (hexokinase 2). Autophagy 2018;14(4):671–84. [PubMed: 28980855]
36. Richard V, Nair MG, Santhosh Kumar TR, Pillai MR. Side Population Cells as Prototype of Chemoresistant, Tumor-Initiating Cells %J BioMed Research International 2013;2013:8.
37. Ciavardelli D, Rossi C, Barcaroli D, Volpe S, Consalvo A, Zucchelli M, et al. Breast cancer stem cells rely on fermentative glycolysis and are sensitive to 2-deoxyglucose treatment. Cell Death Dis 2014;5:e1336. [PubMed: 25032859]
38. Zhou Y, Zhou Y, Shingu T, Feng L, Chen Z, Ogasawara M, et al. Metabolic alterations in highly tumorigenic glioblastoma cells: preference for hypoxia and high dependency on glycolysis. J Biol Chem 2011;286(37):32843–53. [PubMed: 21795717]
39. Liao J, Qian F, Tchabo N, Mhawech-Fauceglia P, Beck A, Qian Z, et al. Ovarian cancer spheroid cells with stem cell-like properties contribute to tumor generation, metastasis and chemotherapy resistance through hypoxia-resistant metabolism. PLoS One 2014;9(1):e84941. [PubMed: 24409314]
40. De Luca A, Fiorillo M, Peiris-Pages M, Ozsvari B, Smith DL, Sanchez-Alvarez R, et al. Mitochondrial biogenesis is required for the anchorage-independent survival and propagation of stem-like cancer cells. Oncotarget 2015;6(17):14777–95. [PubMed: 26087310]
41. Lamb R, Bonuccelli G, Ozsvari B, Peiris-Pages M, Fiorillo M, Smith DL, et al. Mitochondrial mass, a new metabolic biomarker for stem-like cancer cells: Understanding WNT/FGF-driven anabolic signaling. Oncotarget 2015;6(31):30453–71. [PubMed: 26421711]
42. Pasto A, Bellio C, Pilotto G, Ciminale V, Silic-Benussi M, Guzzo G, et al. Cancer stem cells from epithelial ovarian cancer patients privilege oxidative phosphorylation, and resist glucose deprivation. Oncotarget 2014;5(12):4305–19. [PubMed: 24946808]
43. Han S, Wei R, Zhang X, Jiang N, Fan M, Huang JH, et al. CPT1A/2-Mediated FAO Enhancement —A Metabolic Target in Radioresistant Breast Cancer 2019;9(1201).

44. Wang T, Fahrmann JF, Lee H, Li Y-J, Tripathi SC, Yue C, et al. JAK/STAT3-Regulated Fatty Acid β-Oxidation Is Critical for Breast Cancer Stem Cell Self-Renewal and Chemoresistance. Cell metabolism 2018;27(1):136–50.e5. [PubMed: 29249690]

45. Hu J, Li G, Zhang P, Zhuang X, Hu G. A CD44v(+) subpopulation of breast cancer stem-like cells with enhanced lung metastasis capacity. Cell Death Dis 2017;8(3):e2679–e. [PubMed: 28300837]

46. Gao W, Chen L, Ma Z, Du Z, Zhao Z, Hu Z, et al. Isolation and Phenotypic Characterization of Colorectal Cancer Stem Cells With Organ-Specific Metastatic Potential. Gastroenterology 2013;145(3):636–46.e5. [PubMed: 23747337]

47. Doege H, Baillie RA, Ortegon AM, Tsang B, Wu Q, Punreddy S, et al. Targeted deletion of FATP5 reveals multiple functions in liver metabolism: alterations in hepatic lipid homeostasis. Gastroenterology 2006;130(4):1245–58. [PubMed: 16618416]

48. Wang YN, Zeng ZL, Lu J, Wang Y, Liu ZX, He MM, et al. CPT1A-mediated fatty acid oxidation promotes colorectal cancer cell metastasis by inhibiting anoikis. Oncogene 2018;37(46):6025–40. [PubMed: 29995871]

49. Chugh S, Barkeer S, Rachagani S, Nimmakayala RK, Perumal N, Pothuraju R, et al. Disruption of C1galt1 Gene Promotes Development and Metastasis of Pancreatic Adenocarcinomas in Mice. Gastroenterology 2018;155(5):1608–24. [PubMed: 30086262]

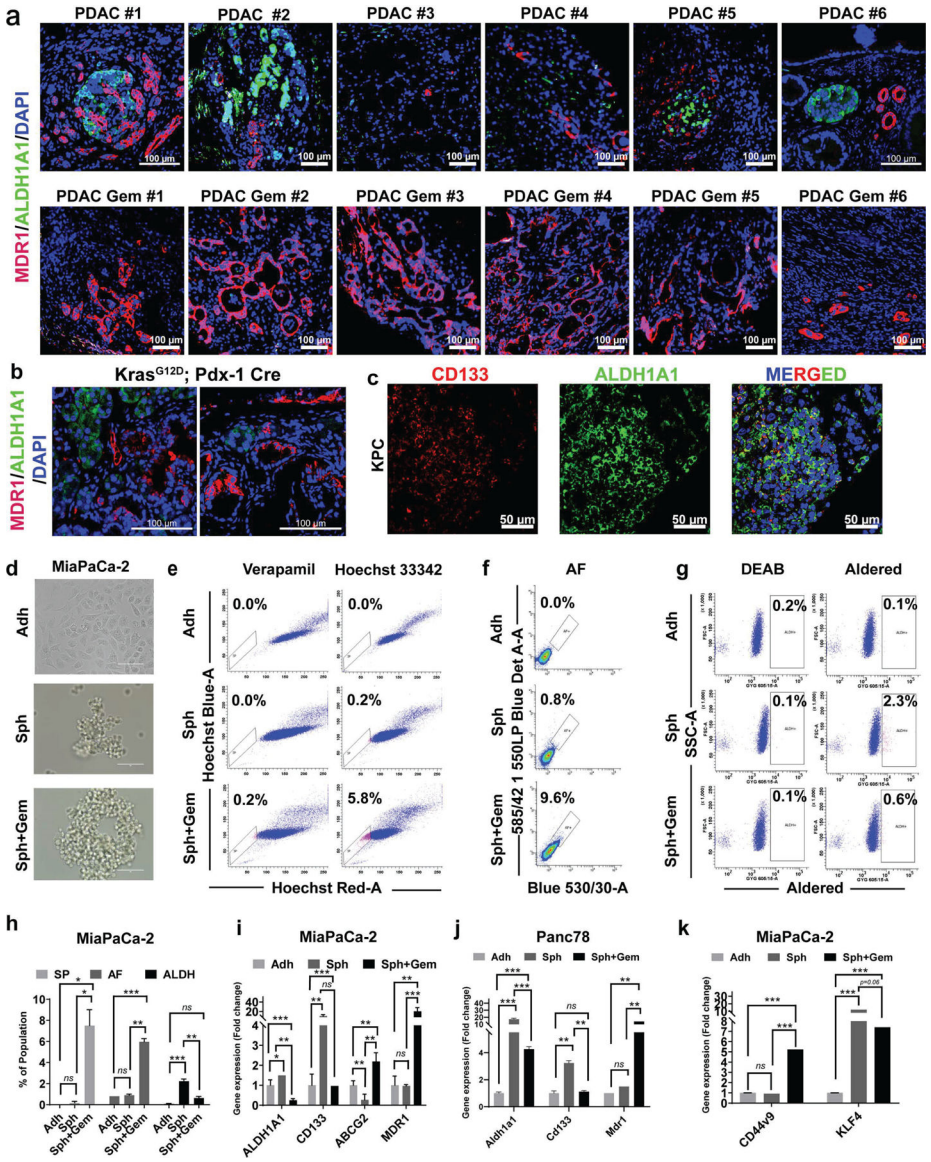

Figure 1. Distinct subtypes of CSC populations in pancreatic cancer show specific stem cell features.

(**a**) Immunofluorescent staining for ALDH1A1 (green) and MDR1 (red) in human pancreas tissues from PDAC patients with or without a history of gemcitabine therapy. Scale bar, 100 µm. (**b**) Immunofluorescent staining for ALDH1A1 (green) and MDR1 (red) in mouse $Kras^{G12D}$; Pdx-1 Cre (KC) pancreatic tissues. Scale bar, 100 µm. (**c**) Confocal microscopy images showing the staining for CD133 (red) and ALDH1A1 (green) in $Kras^{G12D}$; $Trp53^{R172H}$; Pdx-1Cre (KPC) mouse pancreas tissues. Scale bar, 50 µm. (**d**) Light microscopy images showing MiaPaCa-2 (Mia-2) cells enriched in sphere culture conditions with or without gemcitabine (3 µM). The MiaPaCa-2 cells grown in adherent culture were used as a non-CSC control. Scale bar, 50 µm. (**e-h**) Representative flow cytometry plots of side population (SP) assay (e), autofluorescence (AF) assay (f), and aldered assay (g). Percentages of SP, AF, and ALDH+ populations as analyzed by flow cytometry in Adh, Sph, and Sph+Gem cells (h). Data are mean +/− S.D., n = 3. (**i-k**) Real-time PCR analysis

of indicated stem cell markers in adherent culture (Adh), sphere culture (Sph), and sphere culture+gemcitabine (Sph+Gem) of MiaPaCa-2 (i, k) and Panc78 KPC cells (j). Data are mean +/− S.D., n = 3. For all panels, significance was determined with a student's t-test. *p<0.05, **p<0.01, ***p<0.001, ns: non-significant, p>0.05.

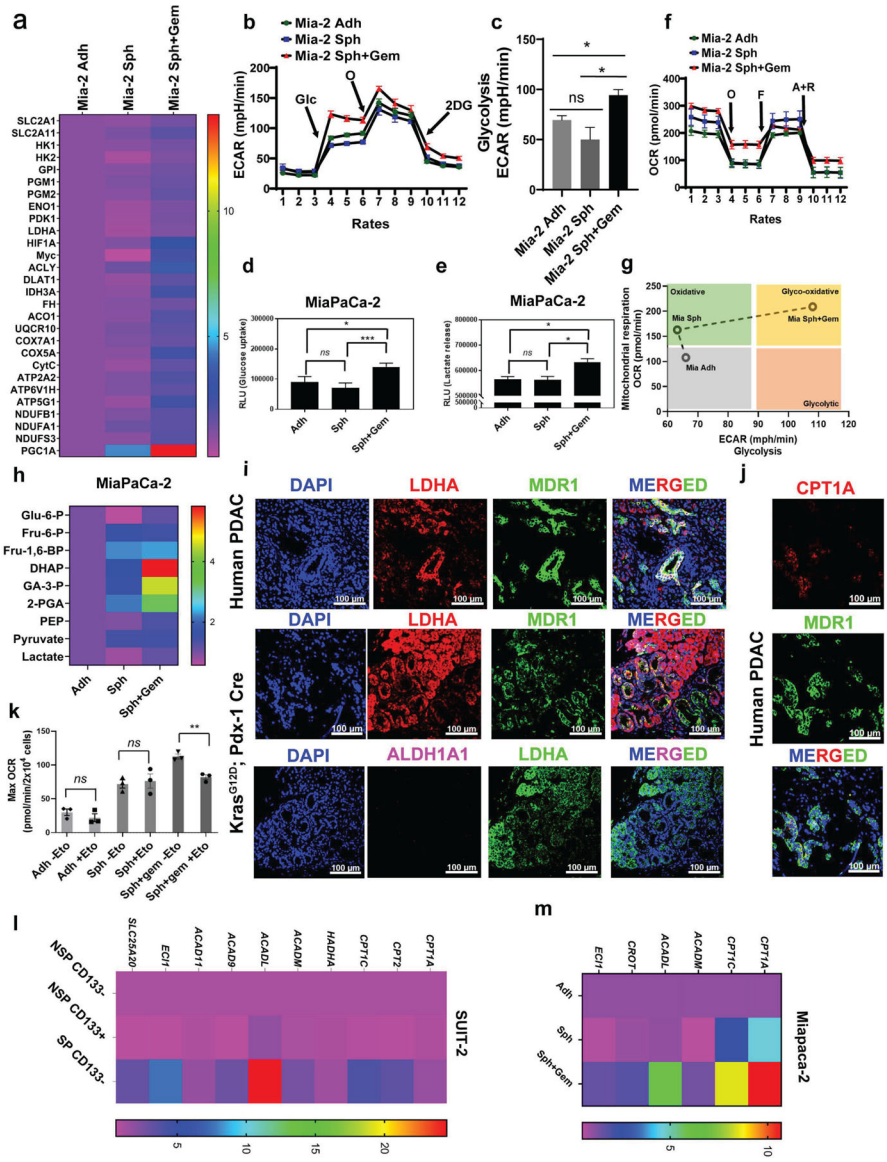

Figure 2. Distinct subtypes of CSC populations show specific metabolic profiles.

(**a**) Heat map showing real-time PCR analysis of energy metabolism (glycolytic and oxidative) genes in MiaPaCa-2 Adh, Sph, and Sph+Gem cells. (n = 3); P<0.05. (**b**) Glycolysis reflected by extracellular acidification rate (ECAR) was measured in MiaPaCa-2 Adh, Sph, and Sph+Gem cells following the addition of glucose (10 mM), oligomycin (1 µM) and 2-deoxyglucose (2-DG) (50 mM). Data are mean +/− S.E.M. n = 6. (**c**) Glycolysis after the addition of glucose. (**d**) Glucose uptake assay. Data are mean +/− S.D., n = 4. (**e**) Lactate release assay. Data are mean +/− S.D., n = 3. (**f**) Oxygen consumption rate (OCR) was measured in MiaPaCa-2 Adh, Sph, and Sph+Gem cells following the addition of oligomycin (1 µM), FCCP (0.5 µM), and electron transport inhibitor, rotenone/antimycin A (0.5 µM). Data are mean +/− S.D., n = 6. (**g**) OCR: ECAR quadrant showing the bioenergetics phenotype of MiaPaCa-2 Adh, Sph, and Sph+Gem cells using the Seahorse analyzer. Data presented as mean ± S.E.M., n = 3. (**h**) Heat map showing relative metabolite

abundance in Adh, Sph, and Sph+Gem cells. n = 3, P<0.05. (**i-j**) Immunofluorescent staining for ALDH1A1, MDR1, LDH-A, and CPT1A in mouse KC and human PDAC pancreas tissues. Scale bar, 100 μm. (**k**) Maximal OCR due to fatty acid oxidation (FAO) as measured by XF Palmitate-BSA FAO Substrate with the XF Cell Mito Stress Test kit using the Seahorse extracellular flux analyzer. Data are mean +/− S.D., n = 3. (**l-m**) Real-time PCR analysis of FAO genes in indicated samples. Data are mean +/− S.D., n = 3. For all panels, significance was determined with a student's t-test. *p<0.05, **p<0.01, ***p<0.001, ns: non-significant, p>0.05.

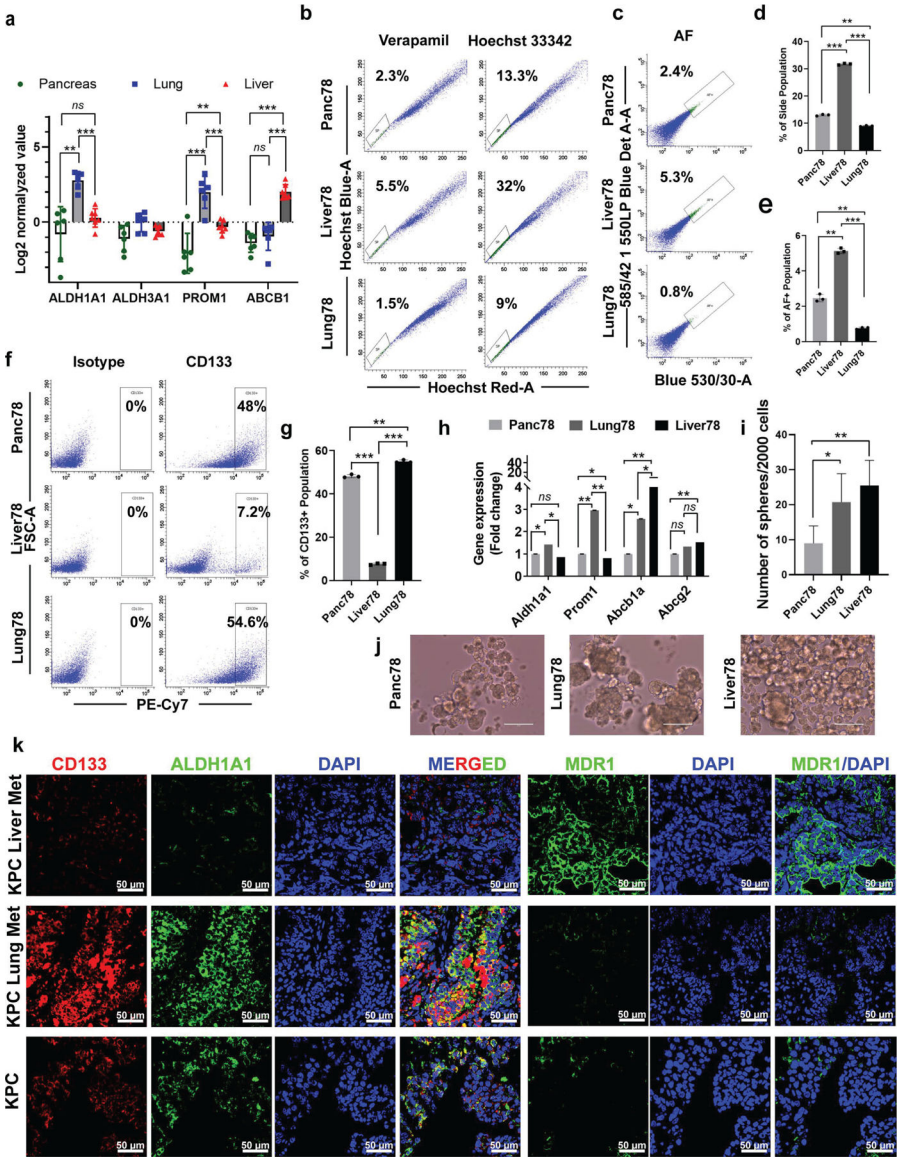

Figure 3. Liver and lung metastasis of PDAC show specific stem cell features.

(a) Analysis of data sets from the GEO database (GSE34153) for the mRNA expression profiles of ALDH1A1, ALDH1A3, PROM1, and ABCB1 in human PDAC primary tumor (n = 7), lung metastasis (n = 6) and liver metastasis (n = 7). Data are mean +/− S.D. (**b-g**) Representative flow cytometry plots of side population (SP) assay (b), autofluorescence (AF) assay (c), and CD133+ cell analysis (f). Percentage of SP (d), AF (e), and CD133+ populations (g) as analyzed by flow cytometry in Panc78, Lung78, and Liver78. Data are mean +/− S.D., n = 3. (**h**) Real-time PCR analysis of indicated stem cell markers in Panc78, Lung78, and Liver78. Data are mean +/− S.D., n = 3. (**i-j**) Sphere formation assay. Bar graph showing the number of spheres per two thousand cells. Spheres >100 µm were counted in four different fields in each group. Data are mean +/− S.D., n = 4. Representative light microscopy images of spheres after ten days post-seeding (j). (**k**) Immunofluorescent staining for indicated markers in KPC primary tumor, KPC-lung metastasis, and KPC-liver

metastasis. Scale bar, 50 μm. For all panels, significance was determined with a student's t-test. *p<0.05, **p<0.01, ***p<0.001, ns: non-significant, p>0.05.

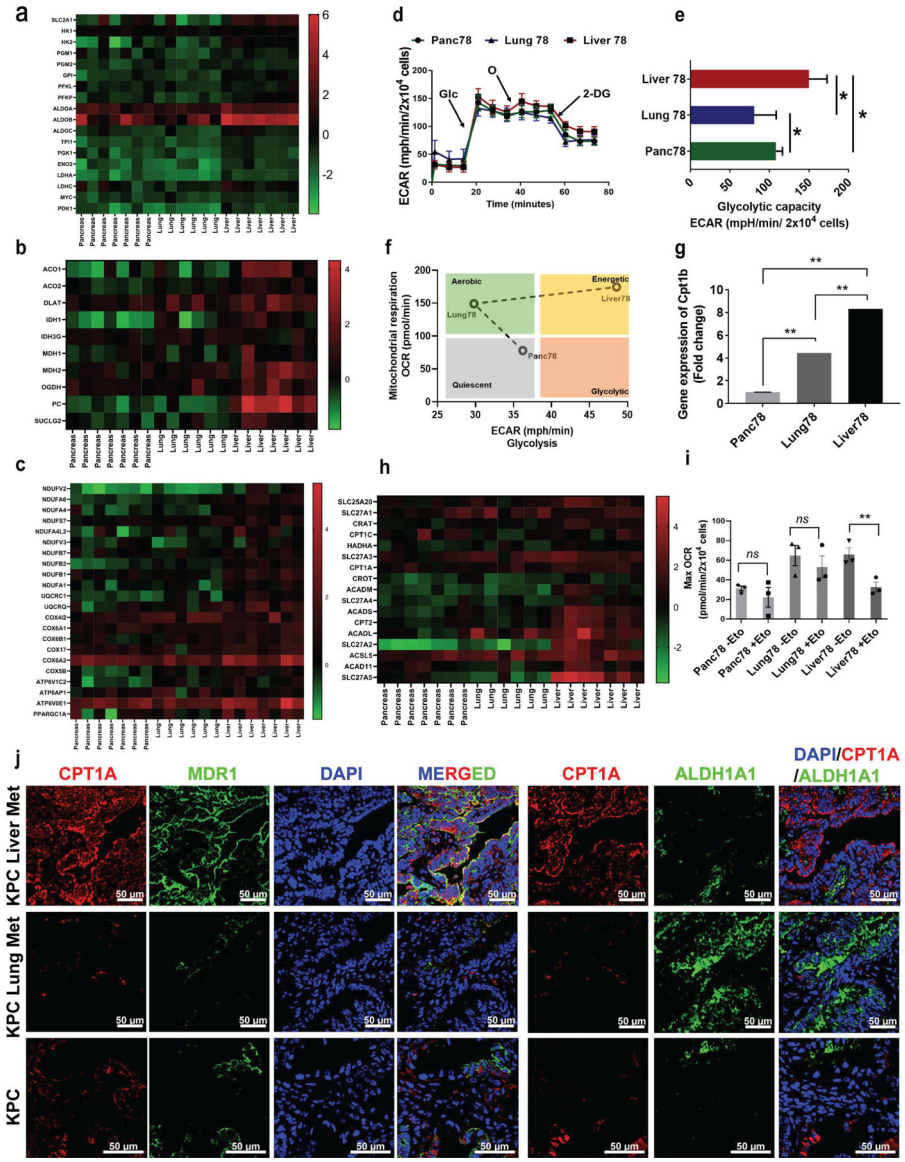

Figure 4. Liver and lung metastases of PDAC show specific metabolic features.

(a-c) Analysis of data sets from the GEO database (GSE34153) for the mRNA expression profiles of glycolysis genes (a), TCA cycle genes (b), and oxidative phosphorylation genes (c) in human PDAC primary tumor (n = 7), lung metastasis (n = 6) and liver metastasis (n = 7). Data are mean +/− S.D. (**d**) Glycolysis reflected by extracellular acidification rate (ECAR) was measured in Panc78, Lung78, and Liver78 following the addition of glucose (10 mM), oligomycin (1 μM) and 2-deoxyglucose (2-DG) (50 mM). Data are mean +/− S.E.M. n = 6. (**e**) Glycolytic capacity as measured from the ECAR values in (d). (**f**) Plot representing the ratio of OCR/ECAR for Panc78, Liver78, and Lung78. (**g**) The real-time PCR analysis of Cpt1b in Panc78, Lung78, and Liver78. Data are mean +/− S.D., n = 3. (**h**) Analysis of data sets from the GEO (GSE34153) for the mRNA expression profiles of fatty acid β-oxidation (FAO) genes in indicated samples. Data are mean +/− S.D. (**i**) Maximal OCR measured by the Seahorse extracellular flux analyzer in the presence and absence

of etomoxir. Data are mean +/− S.D., n = 3. (**j**) Immunofluorescent staining for indicated markers in KPC primary tumor, KPC-lung metastasis, and KPC-liver metastasis. Scale bar, 50 μm. For all panels, significance determined with a student's t-test. *p<0.05, **p<0.01, ***p<0.001, ns: non-significant, p>0.05.

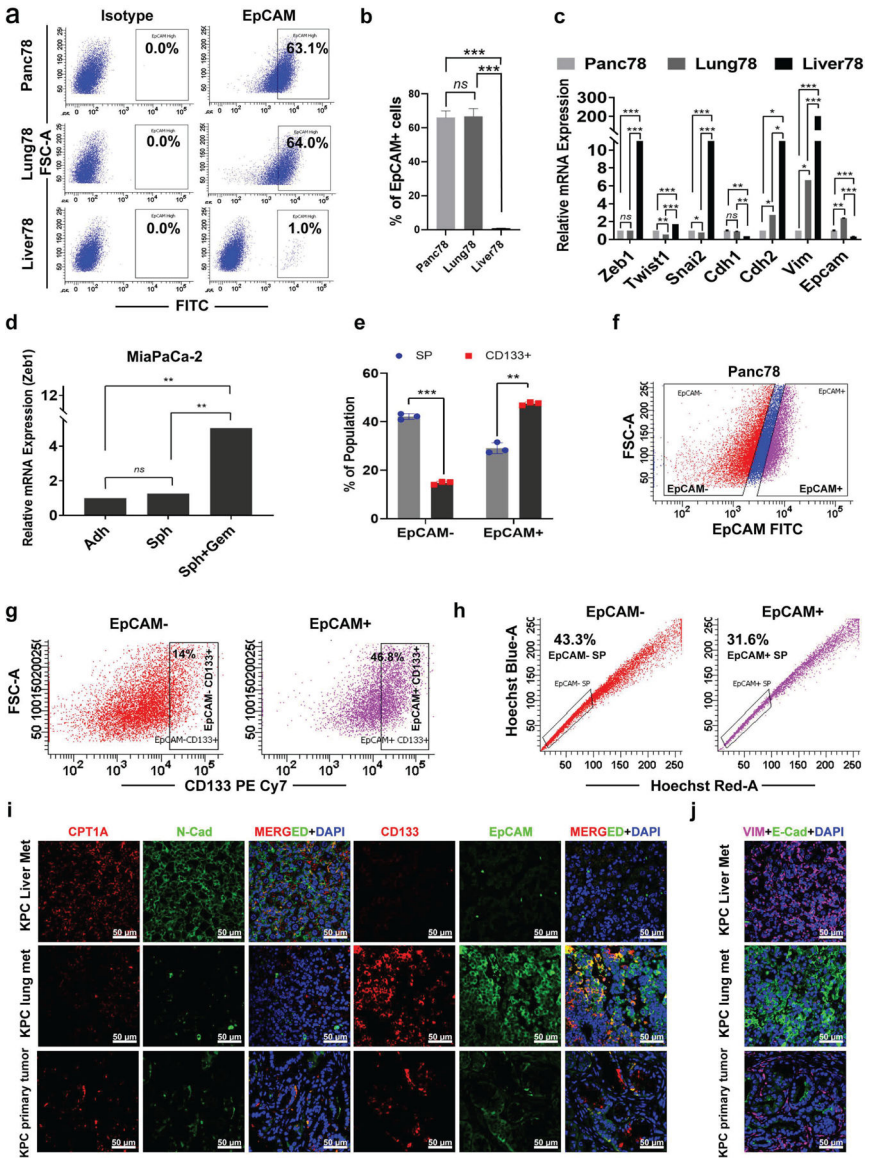

Figure 5. Liver and lung metastases of PDAC show specific EMT/MET features.

(**a-b**) Representative flow cytometry plots of EpCAM+ cell analysis (a). Percentage of the EpCAM+ population as analyzed by flow cytometry in Panc78, Lung78, and Liver78 (b). Data are mean +/− S.D., n = 3. (**c**) Real-time PCR analysis of EMT genes in Panc78, Lung78, and Liver78. Data are mean +/− S.D., n = 3. (**d**) Real-time PCR analysis of Zeb1 in Panc78, Lung78, and Liver78. Data are mean +/− S.D., n = 3. (**e**) Bar graph showing the percentage of SP and CD133+ cells in EpCAM+ and EpCAM− populations in Panc78 cells as analyzed by flow cytometry. Data are mean +/− S.D., n = 3. (**f-h**) Representative flow cytometry plot of EpCAM+ cell analysis in Panc78 (f). EpCAM+ and EpCAM− cells were selected and further analyzed for the percentages of CD133+ cells (g) and SP (h). (**i-j**) Immunofluorescent staining for indicated markers in KPC primary tumor, KPC-lung metastasis, and KPC-liver metastasis. Scale bar, 50 μm. For all panels, significance was

determined with a student's t-test. *p<0.05, **p<0.01, ***p<0.001, ns: non-significant, p>0.05.

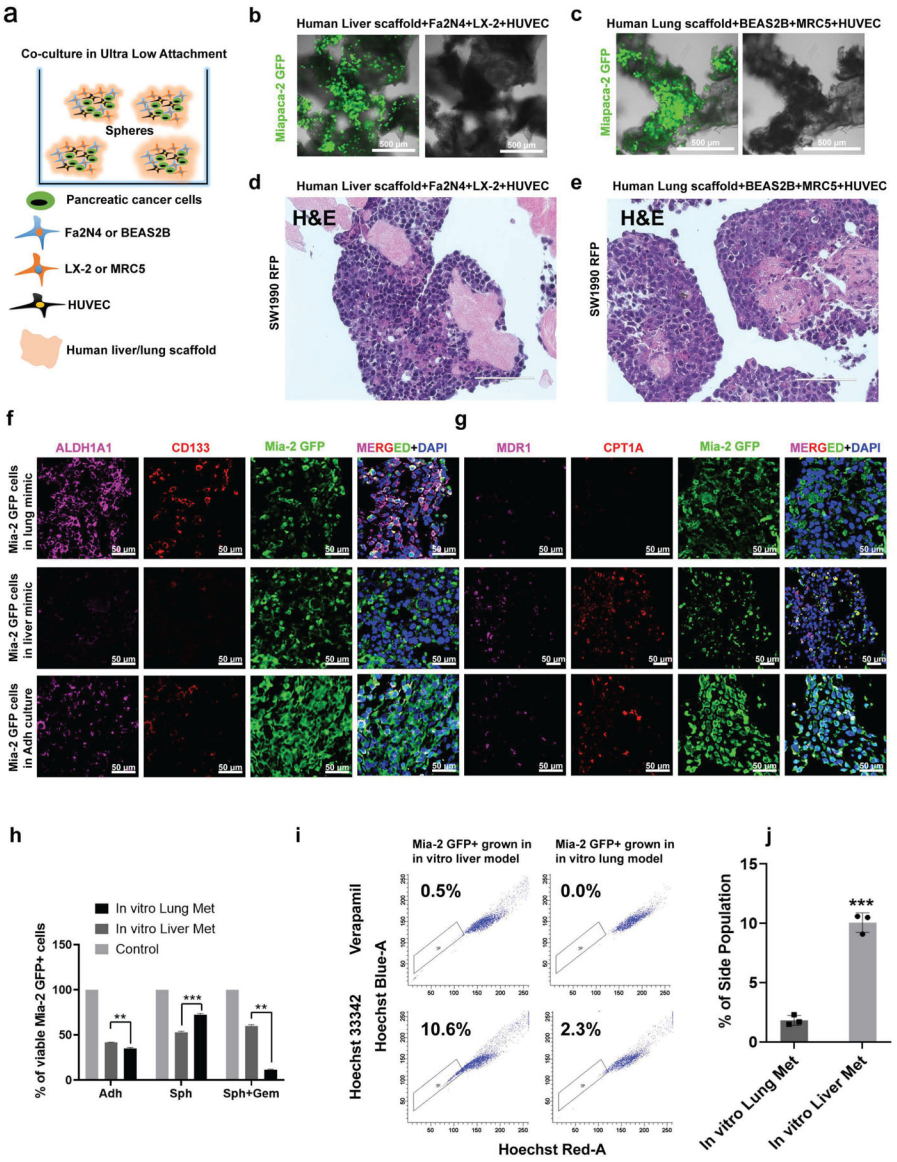

Figure 6. Organ-specific colonization potentials of distinct pancreatic CSCs

(**a**) Schematic showing the strategy of developing “in vitro organ-specific metastasis models”. For liver metastasis, PDAC cells were mixed with Fa2N4, LX-2, HUVEC cells, and human decellularized liver scaffold. For lung metastasis, PDAC cells were mixed with BEAS2B, MRC5, HUVEC cells, and human decellularized lung scaffold. Cells were then cultured in ultra-low attachment plates in DMEM/F12 medium supplemented with B27 and penicillin/streptomycin. (**b,c**) Light microscopy images showing *in vitro* liver and lung metastasis models: MiaPaCa-2 GFP+ cells grown in *in vitro* environments mimicking liver/lung. (**d,e**) H&E staining of *in vitro* liver and lung metastasis models. (**f-g**) Immunofluorescent staining for indicated markers in *in vitro* liver and lung metastasis models. Scale bar, 50 μm. (**h**) Flow cytometry analysis of the percentage of MiaPaCa-2 GFP+ Adh, Sph, and Sph+Gem cells grown in the liver- or lung-mimicking environments. Data are mean +/− S.D., (n = 3). (**i-j**) Representative flow cytometry plots of SP analysis in

MaPaCa-2 GFP+ cells grown in the liver- or lung-mimicking environments (i). Percentage of SP in MaPaCa-2 GFP+ cells grown in the liver- or lung-mimicking environments as analyzed by flow cytometry (**j**). Data are mean +/− S.D., n = 3. For all panels, significance was determined by student's t-test. *p<0.05, **p<0.01, ***p<0.001, ns: non-significant, p>0.05.

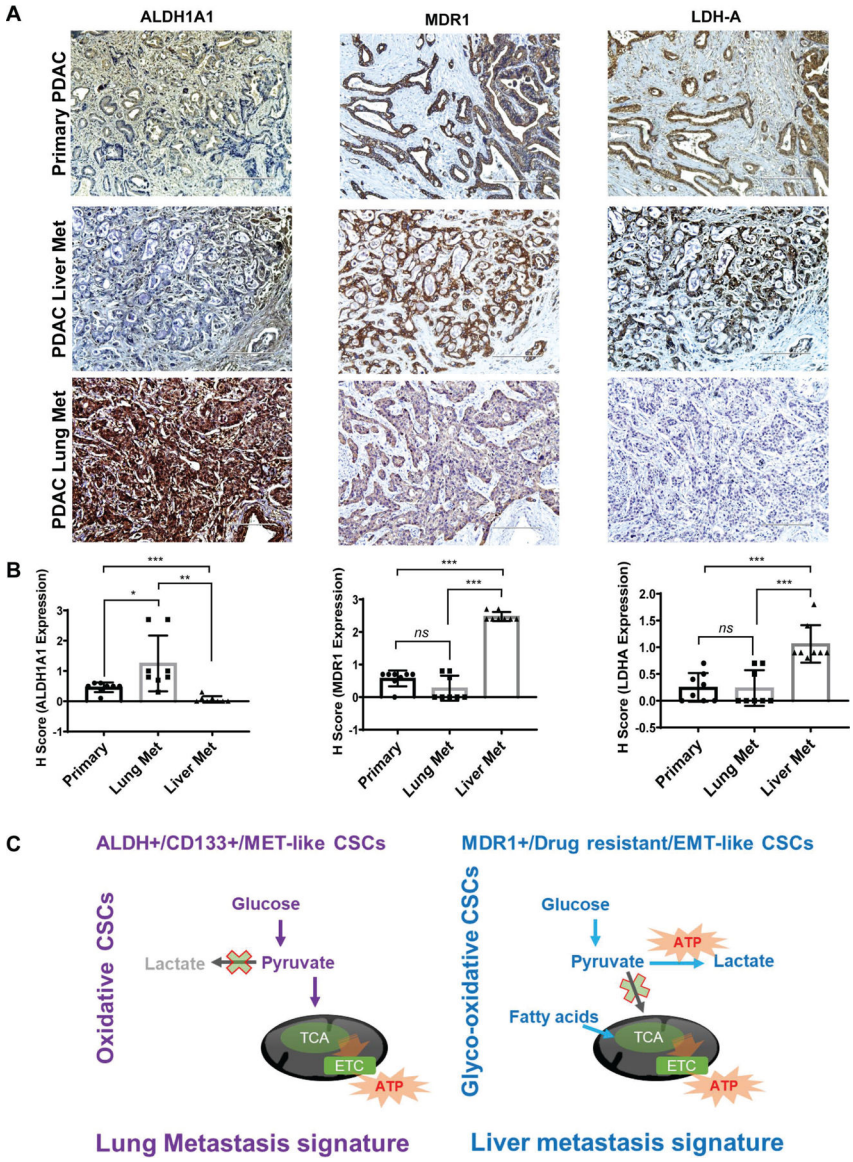

Figure 7. Human PDAC lung and liver metastases show specific stem cell and metabolic profiles relative to primary PDAC.

(a) Representative Immunohistochemistry images of ALDH1A1, MDR1, and LDHA staining in primary PDAC, lung metastasis, and liver metastasis. Scale bar, 200 μm. (**b**) Graphs correspond to the quantification of ALDH1A1, MDR1, and LDHA staining, represented by the H-score. Data are mean +/− S.D., n = 8. For all panels, significance was determined by student's t-test. *p<0.05, **p<0.01, ***p<0.001, ns: non-significant, p>0.05. (**c**) Schematic showing the overall summary of the study.